Journal of Solid Mechanics Vol. 15, No. 2 (2023) pp. 185-197
DOI: 10.22034/jsm.2022.1955820.1738

Research Paper

Vibrational Behavior Study of Effect of Crack on Atomic Force Microscope Cantilever Using a Structural Mechanics Model

E. Kouroshian, V. Parvaneh *, M. Abbasi

Department of Mechanical Engineering, Shahrood Branch, Islamic Azad University, Shahrood, Iran

Received 3 March 2023; accepted 30 April 2023

ABSTRACT

In this research, a multi-scale model was used to analyze the vibrational behavior of the atomic force microscope (AFM) on a graphene sheet sample. Cantilever and silicone tip base were simulated based on the continuum mechanics using finite element modeling and the tip apex were modeled based on the Tersoff potential by the structural mechanics modeling. The contact behavior between the tip and graphene was investigated using measuring friction force during the tip movement on the graphene layer, and its results were compared to the results obtained from molecular dynamics simulation and experimental test. The friction force between the tip and graphene increases by enhancing the tip radius and the contact surface between the tip and the sample. Moreover, the friction force dwindles by heightening the number of graphene layers as a result of sliding graphene layers on each other and diminishing the Poker effect (wrinkling). With the initial distance displacement of the tip from the sample, two curves of the tip vibration amplitude variations and the phase change between tip vibration and excitation vibration were plotted, and the effect of crack and its location in the cantilever was studied. The results showed that the crack in the cantilever can dramatically influence the tip vibration amplitude and the phase change between the tip vibration and the excitation signal.

Keywords: AFM; Cantilever; Crack; Graphene; Structural mechanics.

1 INTRODUCTION

THE atomic force microscope (AFM) is one of the most important instruments used to detect the nanoscale surface properties of the materials [1-5]. AFM is formed of a microscale cantilever and a sharp tip. The tip has usually a few micrometers height and a few nanometers radius in the contact area with the sample, which is utilized

*Corresponding author. Tel.: +98 915 1014452, Fax.: +98 23 3237151.
E-mail address: vali.parvaneh@iau-shahrood.ac.ir (V.Parvaneh)

to scan the surface of the sample. A lot of information about the properties of the surface is achievable by measuring the cantilever vibrations initiated from the interactions between the tip and the sample during moving the tip on the surface. Different models have been recommended to simulate the AFM performance and the vibrational analysis of the cantilever system and the probe of the tip. In most of these models, a system with one or two degrees-of-freedom related to mass-spring-damper was used for the dynamic analysis of the tip [6-9]. Although these models can present acceptable results in some cases, the AFM mechanic behavior is severely under the influence of the tip-sample contact, and this is how models are capable of further precisely simulating the friction behavior and the interaction between the tip and the sample. Meanwhile, the properties of the materials and the geometry of the cantilever and the tip are not considered in these types of models, while they affect the tip movement. The finite element continuous models have been used to simulate the cantilever beam of the AFM. In these models, the cantilever beam is supposed as the Euler-Bernoulli [10-12] or the Timoshenko beam [13-15]. Espinoza-Beltrán et al. used a FEM model for modeling cantilever and silicone tip to simulate vibrational frequencies and determine the contact stiffness of the tip-sample in AFM [16]. Mendles et al. employed a method, which combines the Euler-Bernoulli and Timoshenko beams, to calibrate the spring constants of the AFM cantilever [17]. Using the finite element method, Wang et al. evaluated the hardness and natural frequencies of the cantilever in AFM in addition to the uncertainty in the dimensional parameters and the materials' properties initiated from the manufacturing process [18]. Rodrigues et al. utilized a finite element model to analyze a piezoelectric actuator base-coupled AFM cantilever beam [19]. They used an Euler–Bernoulli beam and Lennard-jones potential to model cantilever and tip-sample interaction, respectively. They also revealed that at least four vibrational mods are required to retain in a reduced-order model. Although the FEM continuous models have suitable simulation speeds and higher time steps, the completely continuous models are not capable of further precisely modeling the effects of complicated boundary conditions in the tip-sample contact. In recent years, to further accurately simulate the tip-sample interaction in AFM, different molecular dynamics methods have been used. In these simulations, only the end part of the tip, which is in contact with the sample, is atomically simulated with a limited number of atoms. Hu et al. utilized molecular dynamics simulation for AM-AFM modeling, which was under the influence of both sinusoidal excitation signal and silicon tip-graphene substrate interactions [20]. A semi-hemisphere tip with a diameter of 3 mm and a height of 1.2 *nm* was considered. In another research, they investigated the effect of size of the AFM tip apex on the topography of the HOPE surface [21]. They increased the tip radius up to 10 nm and showed that the resolution of AM-AFM measurements of atomic steps can have a direct relationship with the tip size. They concluded that the sample deformation and its effect on the contact interaction forces and oscillation amplitude are the reasons, making difference in the experimental and simulation results. In the point of view of the molecular dynamics, Kim et al. used a half-sphere platinum tip contacting a flat surface of the same metal in order to model the dynamic interactions. They realized that nanoscale probes have accurate results just for a small range of indentations large enough (for continuous elasticity) and small enough (for avoiding plastic deformation) [22]. For an interaction between an amorphous silica tip and an amorphous poly-(methyl-methacrylate) substrate, Onofrio et al. utilized the molecular dynamics method proposed by Kim et al. [23]. They modeled a 12 *nm* diameter tip but eliminated the atoms located in the inner shell of the tip to reduce the number of atoms and overcome the time limitation. Ye et al. used molecular dynamics to study the friction behavior of the diamond tip and graphene substrate for a different number of graphene layers [24]. They showed that when the graphene size increases a little bit more than 24 nm, the puckering effect decreases by increasing the number of layers. Dou et al. proposed an atomic model to dynamically analyze a bimodal AFM using molecular dynamics simulation [25]. Unlike the other models, they used double springs and different virtual atoms for modeling the cantilever. Using dual-frequency excitation, they obtained amplitude and phase shift dependency with the average tip-surface distance for the two first vibrational modes. It may be possible some cracks create during the manufacturing process of the AFM cantilever, affecting the performance of the microscope. Few studies were conducted on the AFM vibrational analysis with a cracked cantilever. The primary investigations were conducted by Lee and Chang [26, 27]. They examined the sensitivity of the AFM flexural vibrations having a crack using a theoretical model and considering two normal and lateral springs for the tip-sample interaction and a rotational spring for modeling crack in the cantilever. They showed that when the contact stiffness is low, the sensitivities of the three first modes of the cracked cantilever are higher than those of the non-cracked cantilever; this is vice versa when the contact stiffness is high. In another research, they examined the vibrational behavior of the AFM cracked cantilever in a machining process. Their results indicated that the vibration displacement of the cracked cantilever is remarkable, especially when the crack is close to the fixed end of the cantilever. Moreover, this displacement becomes more by increasing the crack flexibility. They also worked on another project and indicated that the modal sensitivity obtained using the modified couple stress theory is lower than the classical beam theory for contact stiffness [28]. Dastjerdi et al. examined the vibrational behavior of the AFM cracked cantilever using the matrix transfer model and modeling crack in the form of a torsional spring [29].

Their results showed that the maximum values will be obtained for sensitivity and natural frequency in the first and second modes. They also concluded that, in the soft samples, the crack growth leads to reducing sensitivity; however, this is vice versa in the stiff samples.

In this research, a structural mechanic model was used for analyzing the vibrational behavior of the cracked cantilever AFM. The tip-sample interaction was modeled using nonlinear springs, which follow the Lennard-Jones potential. The desired sample is a graphene sheet with a maximum of three layers; this sheet was located on a silicon substrate and was modeled using the modified Morse potential. The tip apex, which is in contact with the sample surface, was atomically modeled using the Tersoff potential. The other parts of the tip and the cantilever were simulated using a finite element model. To validate the friction and displacement values, the results were compared to the experiments and dynamics molecular models. Moreover, the effect of crack and its different locations in the cantilever on the AFM vibrational behavior was investigated.

2 METHODS

2.1 Computational details

At first, a structural model of graphene sheet is created to simulate the vibrational behavior of the AFM and study the friction between graphene and microscope tip. In fact, it is obvious that there are some similarities between the molecular model of a graphene sheet and the structure of a frame. In a graphene sheet, carbon atoms are bonded together by covalent bonds. These bonds have their characteristic bond lengths and bond angles in a three-dimensional space. Thus, it is logical to simulate the deformation of a graphene sheet based on the method of classical structural mechanics. From the structural characteristics of graphene sheet, it is logical to anticipate that there are potential relations between the deformations of graphene sheet and frame-like structures. For macroscopic space frame structures made of practical engineering materials, the material properties and element sectional parameters can be easily obtained from material data handbooks and calculations based on the element sectional dimensions. For nanoscopic graphene sheet, there is no information about the elastic and sectional properties of the carbon-carbon bonds and the material properties. Therefore, it is imperative to establish a linkage between the microscopic computational chemistry and the macroscopic structural mechanics. The carbon atoms were arranged in the form of a hexagon in the graphene sheet, and there are different kinds of interactions between these atoms (Fig. 1). The total potential energy of carbon atoms is expressed as follows:

$$U_{total} = U_r + U_\theta + U_\omega + U_\phi + U_{vdw} + U_{el} \tag{1}$$

where $U_r + U_\theta + U_\omega + U_\phi + U_{vdw}$, and U_{el} denote the bond stretching, the bond angle variations, dihedral angle torsion, out-of-plane torsion, van der Waals, and electrostatic, respectively. In this simulation, the electrostatic energy U_{el} was overlooked because of its negligible value in comparison with the other bond energies. Likewise, the van der Waals energy, which is related to the non-bonding atoms in modeling single-layer graphene sheet, was neglected due to its insignificant value compared to the bonding energies, but, for modeling multilayer graphene sheets, it was used to simulate the interaction between graphene layers. The equations corresponding with these bonding energies are considered as follows:

$$U_r = D_e \left\{ \left[1 - e^{-\beta(r - r_0)} \right]^2 - 1 \right\} \tag{2}$$

$$U_\theta = \frac{1}{2} K_\theta \left(\theta - \theta_0 \right)^2 \left[1 + K_{sextic} \left(\theta - \theta_0 \right)^4 \right] \tag{3}$$

$$U_\phi = \frac{1}{2} K_\phi \left[1 + \cos\left(n\phi - \phi_0 \right) \right] \tag{4}$$

$$U_\omega = \frac{1}{2} K_\omega \left[1 + \cos\left(n\omega - \omega_0 \right) \right] \tag{5}$$

$$U_{vdw} = 4\varepsilon\left[\left(\frac{\sigma}{r}\right)^{12} - \left(\frac{\sigma}{r}\right)^{6}\right] \tag{6}$$

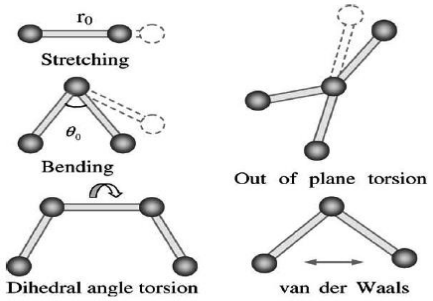

Fig.1
Interatomic interactions in molecular mechanics.

The constants used in the equations above are presented in Table 1.

Table 1
The constants of interaction equations in the graphene sheet.

Interaction	Parameters
U_r	$D_e = 0.6031nN.nm, \beta = 26.25nm^{-1}, r_0 = 0.142nm$
U_θ	$K_\theta = 1.42\frac{nNnm}{Rad^{-2}}, K_{sextic} = 0.75Rad^{-4}, \theta_0 = 120^\circ$
U_ϕ	$K_\phi = 0.278\frac{nNnm}{Rad^{-2}}, n = 2, \phi_0 = 180^\circ$
U_ω	$K_\omega = 0.278\frac{nNnm}{Rad^{-2}}, n = 2, \omega_0 = 180^\circ$
U_{vdw}	$\varepsilon = 2.84meV, \sigma = 0.34nm$

Axial springs were utilized to model the variation of the bonding angle between carbon atoms (see Fig. 2(a)). The relation between the bond angle variations ($\theta\Delta$) and the corresponding length variations (ΔR) is expressed as below:

$$\Delta\theta \approx \frac{2(\Delta R)}{r_0}, r_0 = 0.142nm \tag{7}$$

Therefore, Eq. (3) can be easily rewritten as follows:

$$U_\theta = \frac{2}{r_0^2}K_\theta\left(R - R_0\right)^2\left[1 + \frac{16}{r_0^2}K_{sextic}\left(R - R_0\right)^4\right] \tag{8}$$

The forces and torques between carbon atoms can be obtained through deriving from the aforementioned energy equations:

$$F\left(r - r_0\right) = 2\beta D_e\left[1 - e^{-\beta(r-r_0)}\right]^2 e^{-\beta(r-r_0)} \tag{9}$$

$$F\left(R - R_0\right) = \frac{4}{r_0^2}K_\theta\left(R - R_0\right)^2\left[1 + \frac{48}{r_0^4}K_{sextic}\left(R - R_0\right)^4\right] \tag{10}$$

$$T\left(\phi-\phi_0\right)=\frac{1}{2}K_\phi n\sin\left(n\phi-\phi_0\right) \tag{11}$$

$$T\left(\omega-\omega_0\right)=\frac{1}{2}K_\omega n\sin\left(n\omega-\omega_0\right) \tag{12}$$

$$F_{vdw}\left(r\right)=\frac{4\varepsilon}{r}\left[-12\left(\frac{\sigma}{r}\right)^{12}-\left(\frac{\sigma}{r}\right)^{6}\right] \tag{13}$$

To model the bond stretching, dihedral angle torsion, and out-of-plane torsion, the connector element was used. Moreover, the spring element was utilized to model the interactions of bond angle variations and van der Waals. Both spring and connectors elements used between carbon atoms are nonlinear and their arrangement is observed in Fig. 2(c). A local coordinate system is set at the center of each carbon atom (see Fig. 2(b)); the *x* and *z* directions of the coordinate system are in the direction perpendicular to the graphene sheet.

In this paper, the graphene sheet was simulated to a maximum of three layers. The distance between the layers is equal to 0.34 *nm*, and the interaction between two graphene layers is assumed to be van der Waals. The van der Waals forces can act as attraction and repulsive between carbon atoms. For this purpose, a nonlinear spring element was used based on the Lennard-Jones potential [30].

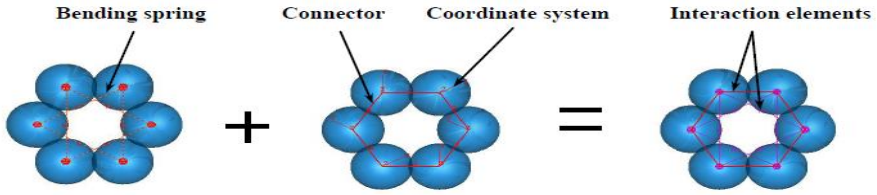

Fig.2
The spring and connector elements corresponding to the interactions between carbon atoms.

The graphene sheet was considered as a square with a dimension of $25\times25nm$, approximately. Graphene sheet was located on a silicone substrate and its all-around was fixed in the plane directions (along the *x* and *y*-directions) (see Fig. 3(a)). To interact between the microscope silicon tip and the graphene sheet, nonlinear springs, which follow the Lennard-Jones potential, were utilized. The LJ parameters for Si-C bond were considered equivalent to $\varepsilon = 8.909\ meV$ and $\sigma = 0.3326\ nm$; these have been employed in recent reports [31]. The cut-off distances of the LJ potential for C-C and Si-C interactions are 1.19 *nm* [32] and 0.8315 *nm* [31], respectively.

The cantilever finite element model is a simulated sample of AFM (XE 100, Park Scientific Instruments) made of South Korea. It has a silicon tip with a length of 15 μm and a radius of 16 *nm* (Mikromasch, NCS36). The thickness and length of the cantilever are equal to 1 μm and 130 μm, respectively.

An atomic structural mechanic model was used in the tip apex for more accuracy in interactions of the tip with the graphene sheet (see Fig. 3(b)). In this model, Si-Si bonds follow the Tersoff many-body potential function:

$$V_{ij}=f_c\left(r_{ij}\right)\left[A_{ij}\exp\left(-\lambda^{(1)}r_{ij}\right)-Bb_{ij}\exp\left(-\lambda^{(2)}r_{ij}\right)\right] \tag{14}$$

where f_c is a cut-off function, which restrains the potential amplitude and expresses as follows:

$$f_c\left(r_{ij}\right)=\begin{cases}1, & r_{ij}\prec R^{(1)}\\ \frac{1}{2}+\frac{1}{2}\cos\frac{\pi\left(r_{ij}-R^{(1)}\right)}{\left(R^{(2)}-R^{(1)}\right)}, & R^{(1)}\prec r_{ij}\prec R^{(2)}\\ 0, & r_{ij}\succ R^{(2)}\end{cases} \tag{15}$$

b_{ij} is the many-body bond order parameter describing the bond energy formation (attractive part of the potential V_{ij}) in the case of the local atomic arrangement due to the presence of other neighboring atoms:

$$b_{ij} = \left(1+\beta^n \xi_{ij}^n\right)^{-1/2n} \tag{16}$$

ξ is the effective harmony number, which is defined as follows:

$$\xi_{ij} = \sum_{k\neq i,j} f_c\left(r_{ij}\right) g\left(\theta_{ijk}\right) \tag{17}$$

$g(\theta_{ijk})$ is the bonding angle function between *i-j* and *i-k* bonds. This function is defined as follows:

$$g\left(\theta_{ijk}\right) = 1+\frac{c^2}{d^2}+\frac{c^2}{\left[d^2+\left(h-\cos\theta_{ijk}\right)^2\right]} \tag{18}$$

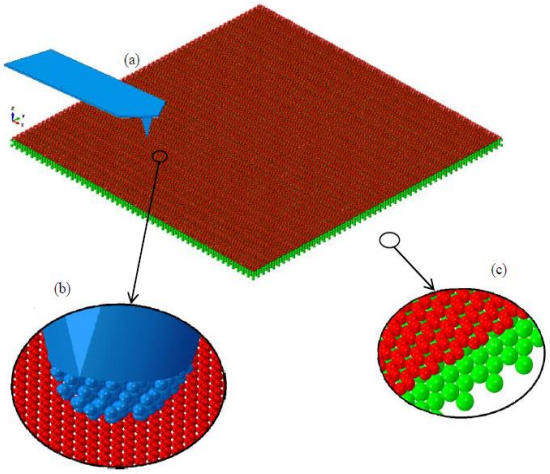

Fig.3
A schematic of the multiscale model of AFM and graphene sheet with a silicone substrate.

The parameters related to the Tersoff potential for the Si-Si bond at the silicone tip are presented in Table 2. Due to the high time and cost required for the atomic modeling of the microscope silicone tip, which is in the range of micrometer, in this model, therefore, the tip apex was simulated to a maximum height of 8 *nm* and diameter of 16 *nm* (under the influence of interaction with graphene sheet) using an atomic structural mechanic model, and then it was connected to a continuous finite element model.

A 20N normal force was applied by the tip to contact the graphene sheet. The substrate was moved with a constant rate of 0.01 *nm/ps* along the graphene sheet and in two different directions of zigzag and armature. Therefore, the tip was deflected because of the van der Waals forces, and the friction force can be obtained using simulation.

Table 2
Tersoff potential parameters for the interaction in the Si-Si bond.

Parameter	$A(eV)$	$B(eV)$	$\lambda^{(1)}(nm^{-1})$	$\lambda^{(2)}(nm^{-1})$	n	c
	1830.8	471.18	2.4799	1.7322	0.78734	1.0039×10^5
Parameter	d	$R^{(1)}(nm)$	$R^{(2)}(nm)$	β	h	
	16.217	0.27	0.30	1.1×10^{-6}	-0.59825	

2.2 Finite element modeling

Presence of crack causes a complex geometrical property which is difficult to study. So finite element method (FEM) is used and for finite element analysis (FEA), ABAQUS has been used. In the present work, the behavior of

crack on the AFM cantilever was simulated using extended finite element method (XFEM). In conventional FEM, cracks or any other discontinuity are defined as an intrinsic part of the finite element mesh and are modelled by aligning the element boundary with the crack geometry. So, when the crack tip advances, the mesh must be redefined to ensure this alignment. In XFEM approach, the crack is independent of mesh, and hence, a crack can propagate through elements without remeshing. This significantly reduces the computational resources. There are two commonly used elements for meshing 3D models: the brick element and the tetrahedron element. It has been documented that brick elements can show better performance compared with the tetrahedron. However, for the cases of complex geometries, the probability of geometry degradation exists when meshing the model with brick elements. In addition, the number of nodes of brick elements is higher than the number of elements which significantly increases the computational time. Re-meshing of the brick elements is difficult and hence may not be suitable for large deformation problems. Therefore, the tetrahedron element, the 10-node quadratic tetrahedron (C3D10), was adopted for the numerical model of this study (See Fig. 4). To find the appropriate mesh size, the convergence study was performed and the corresponding graph is illustrated in Fig. 5. It can be seen from Fig. 5 that as the size of elements increases the convergence of the results decreases such that after the size of 3.0, the rate of divergence exponentially increases. In this study, to achieve reliable results, the global size of 0.65 was adopted for the mesh size. The number of meshes with this global size is equal to 123661.

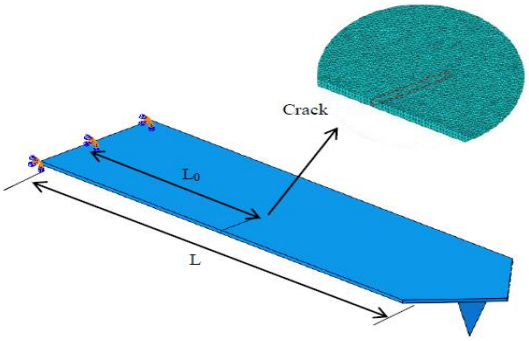

Fig.4
The crack length and situations in the cantilever.

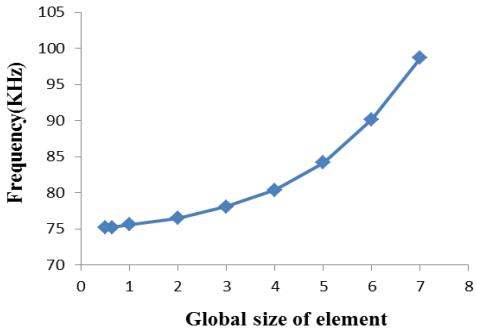

Fig.5
The effect of global size of elements on the frequency analysis of the cantilever.

3 RESULTS AND DISCUSSION

3.1 Friction measurement

The friction values for two zigzag and armature types of the graphene sheet were compared to the results obtained from the molecular dynamics simulation and the experimental results [33] (see Fig. 6). In the molecular dynamics simulation, the maximum radius of the tip apex was considered 2.4 *nm* due to the limitation in the tip dimensions, while the radius of AFM tip apex is a 16 *nm* in a factual condition. To simultaneously compare the structural mechanic model to the molecular dynamics simulation and the experimental results [33], the tip radius changes from the lowest value (1.2 *nm*) to the highest one (16 *nm*) in the current model. As indicated in Fig. 3, the friction in the experimental test is more than the molecular dynamics simulation. Friction is proportional to the contact area at the nanoscale so that the larger the contact area lead to the higher the friction value. The molecular dynamics simulation results were obtained based on a 1.2 *nm* tip radius and are very lower in comparison with a 16 *nm* tip radius in the FFM experiment. Hence, a lower contact area is created in the molecular simulation compared to the FFM

experiment. Additionally, the wrinkling effect of the graphene layer on the molecular simulation is ignored because of the rigidity of the graphene layer [33]. The wrinkling effect in the experimental test results in creating a bigger contact surface and more friction force. Therefore, as a whole, the friction force in the molecular dynamics simulation is smaller in total compared to the friction force belonging to the experimental test. Thus, in present model, flexible graphene and a radius of tip apex similar to the FFM were used. As can be seen, by increasing the tip radius up to 16 nm, the friction force in the structural mechanic model heightens and closes to the friction force obtained by the experimental test. It should be paid attention that the friction obtained by the structural mechanics model is 15% lower than the experimental test. The real graphene layer is not usually flat completely in the initial state and has some wrinkles, and the presence of structural defects in the graphene layer during implementing the experimental test strengthens wrinkling as well. Therefore, it is expected the contact area of the tip and graphene layer in the experimental test is more than the simulation condition. Meanwhile, in the present model, temperature effects, which may affect the friction force, were neglected.

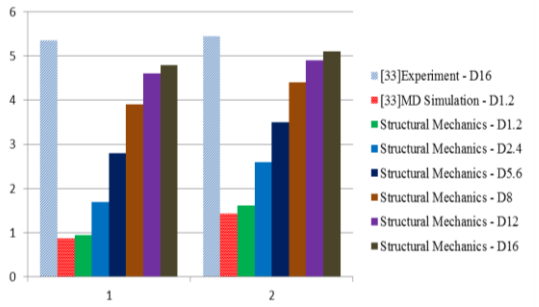

Fig.6
The friction of the AFM tip and graphene sheet in two different directions of zigzag and armchair.

The graphene friction values with different layers were examined for a maximum of three layers. Based on Fig. 7, the friction force decreases slightly by increasing the number of graphene layers. It should be mentioned that this reduction becomes lower by increasing the number of layers. Therefore, the friction also reduces by lowering the wrinkling effect and the contact area reduction of the tip with the graphene layer. The comparison of the results with the molecular dynamics simulation confirms this reducing trend with increasing the number of graphene layers. While the graphene sheet was flexible, the variation in friction is relatively large compared to that in rigid graphene because of the puckering of graphene and the strong adhesion between the tip apex and graphene layer [33].

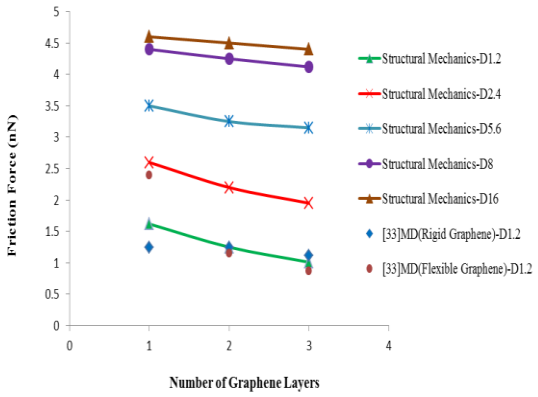

Fig.7
The friction of the AFM tip and graphene sheet with a different number of layers.

The friction force in terms of time for the tip apexes with different radiuses (from 1.2 *nm* to 16 *nm*) is illustrated in Fig. 8. In the simulation, the difference in the contact area leads to creating different contact geometry and energy states for different sizes of the tip. Meanwhile, the tip movement on the graphene layer affects by two different modes of adhesion and sliding due to the honeycomb lattice of the graphene. Hence, the friction force diagram in terms of time has ups (adhesion mode) and downs (sliding mode). Established upon the friction force diagram, there is a good agreement between the results obtained by the structural mechanics model for the lowest tip radius, i.e., 1.2 *nm*, with those obtained from the molecular dynamics simulation. By increasing the tip radius, it is observed that the ups and downs in the friction-time diagram reduce so that the difference between the friction force in the adhesion and sliding modes can be overlooked by increasing the tip radius higher than 5.6 *nm*.

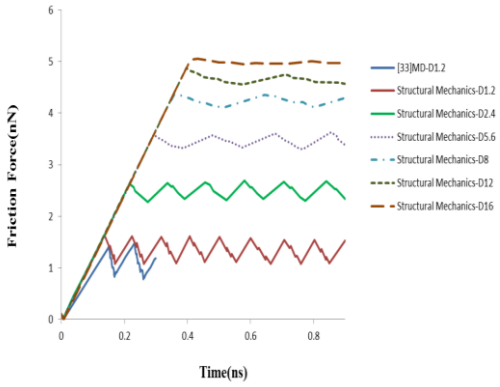

Fig.8
The effect of different radiuses of the tip apex on the friction between the tip and the sample.

3.2 Amplitude analysis

The tip oscillation amplitude and the phase shift between the tip oscillation and excitation signal are two important typically parameters, which are ordinarily measured in the AM-AFM [20, 34]. A virtual atom usually is used instead of the base of the AFM cantilever in the molecular dynamics simulation [20]. In these types of simulations, the virtual atom is connected through a harmonic spring with a certain amount of stiffness in the z-direction (vertical direction to the sample) to the tip apex. The initial distance between the virtual atom and the sample surface is identified as z_c. The virtual atom vibrates with a sinusoidal excitation signal, and the excitation frequency is usually selected close to the natural frequency of the tip. In some of the molecular dynamics simulations, two virtual atoms are employed for the simulation of the cantilever base and the second mode part [25]. In these simulations, the cantilever virtual atom is connected through a harmonic spring to the second virtual atom, and the last one is connected to the tip apex through another spring. Therefore, the bimodal AFM tip is formed and one can adjust two resonance frequencies concerning the system with changing the mass of atoms and stiffness of springs.

In the simulation, the tip oscillation amplitude and the phase shift between the tip oscillation and excitation signal were obtained from the oscillating displacement of the cantilever and the tip. A representative result displaying the time variation of the displacement of the cantilever and the tip is shown in Fig. 9. The tip position z can be described by the equation $z = z_0 + A\ sin\ (w_{tip}\ t - \phi)$, where z_0 is the average tip-sample separation, A is the amplitude of tip oscillation, which is dependent on the angular frequency of the excitation signal w, ϕ is the phase shift compared to excitation signal, and w_{tip} is the angular frequency of tip oscillation, which is determined by w, i.e., $w_{tip} = w$. A sine function was fit to the two waveforms generated by the simulation to obtain the amplitude A and phase shift ϕ. To obtain statistically relevant fits for these values, ten oscillation cycles for both the cantilever and tip displacement were acquired in the simulation and subsequently fit with the sine waveform. Since z_0 was obtained from the fit, the results reported in subsequent sections are in terms of z_c, the initial tip–sample distance, since the latter was the parameter specified in our simulation.

In the structural mechanics simulation, the cantilever base vibrates by a sinusoidal excitation signal with two natural frequencies of 75.2 *kHz* (first mode) and 470.5 *kHz* (second mode).

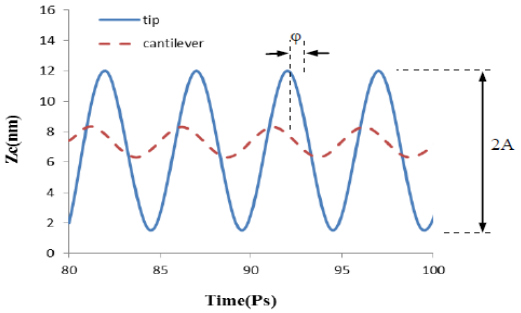

Fig.9
The time-dependent vertical displacement of the cantilever (red dashed line) and the tip (blue solid line) at z_c equal to 7.5 *nm*.

The initial distance between the cantilever base and the surface sample (z_c) is equal to 5.5 *nm*. Fig. 10 and Fig. 11 show the oscillation amplitude (A) and phase shift (φ) diagrams in terms of the tip-sample distance variations. Both diagrams have a pick point at z_c equivalent 9.5 *nm*, indicating the boundary between the attraction and repulsion of

the tip by the sample. By reducing z_c, i.e., lowering the tip-sample distance, the displacement of the tip is highly affected via the tip-sample interaction forces and leads to reducing the oscillation amplitude (Fig. 10). However, by increasing z_c more than 9.5 *nm*, the tip-sample interaction weakens, and the tip only vibrates under the influence of the excitation signal. Therefore, the oscillation amplitude reaches an initial constant value of 7.5 *nm*. In this situation, the dynamic response of the tip is determined using the excitation signal. The trend of the results is similar in comparison with the molecular dynamics simulation. However, the results obtained from the structural mechanics model show lower values compared to the molecular dynamics simulation. This difference is because of the bigger radius of the tip apex in the structural mechanic model compared to the molecular dynamics simulation. The larger surface of the tip-sample interaction in the structural mechanics model leads to reducing the oscillation amplitude of the tip.

The diagram presented in Fig. 11 shows that the two curves of phase shift and oscillation amplitude are in accordance. The phase shift in z_c equivalent to 9.5 *nm* causes a severe discontinuity and changes above 90°. The phase shift is reduced by decreasing z_c in the repulsion regime, but eventually, when the tip is far enough away from the sample and close to the excitation amplitude, it leans toward a constant value of 91°. As recommended in the literature, the phase shift between the drive and the cantilever amplitude signal should be less and more than 90° for the system that works in the repulsion and attraction forces [34, 35].

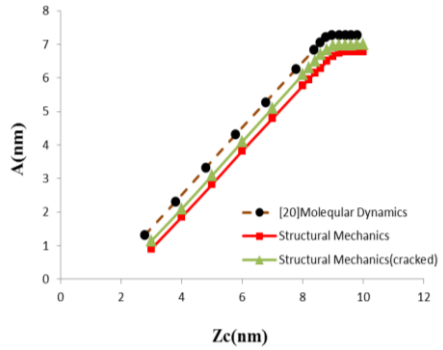

Fig.10
The oscillation amplitude of the tip in terms of z_c.

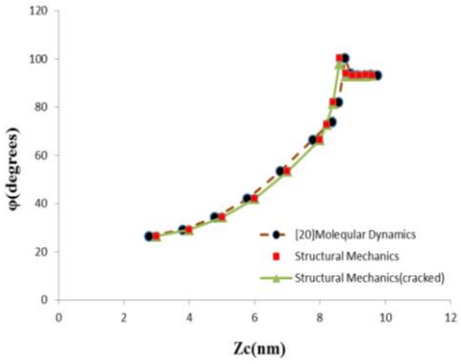

Fig.11
The phase shift between the tip and cantilever in terms of z_c.

In order to investigate the effect of crack in the cantilever on the oscillation amplitude of the tip, the results are compared for cracked and non-cracked cantilever conditions. Crack was created in three different situations (nearby the free side (L_0/L=0.2), middle (L_0/L=0.5), and nearby the fixed side (L_0/L=0.8)) in the cantilever and then compared to each other (Fig. 12). The crack length is equal to one-third of the width of the cantilever (the width of the cantilever is equal to 32.5μm). The comparison between the curves shows that the maximum effect on the tip vibration occurs compared to the two other conditions (middle of the cantilever and nearby the tip) when the crack is close to the support. As can be seen, the oscillation amplitude of the tip in the cracked cantilever becomes more compared to the non-cracked condition. It should be noted this increase in oscillation amplitude of the tip reduces by decreasing z_c. Therefore, when the interaction amongst the tip and graphene is of repulsion type, the effect of crack is less; however, this effect becomes more by changing the regime from repulsion to attraction.

Crack in the cantilever also affects phase shift so that, at the maximum condition when the crack is close to the support of the cantilever, the phase shift occurs at the lower z_c compared to the non-cracked condition, i.e., 8.25 *nm* (Fig. 13). This indicates that the repulsion-to-attraction regime change occurs at a lower distance of the sample (lower z_c). This conclusion is also valid for the oscillation amplitude (Fig. 12).

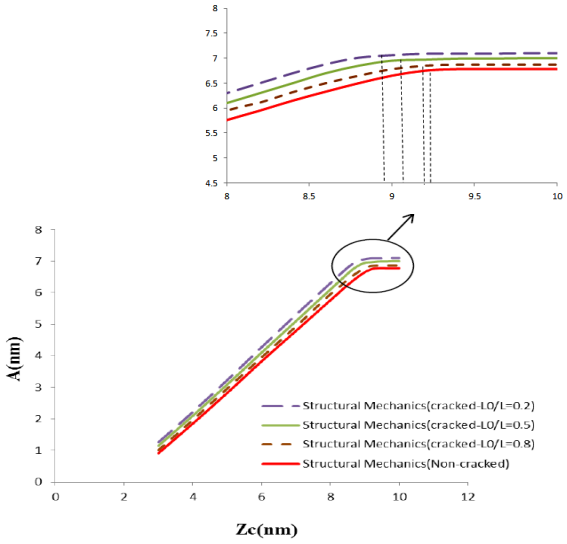

Fig.12
Comparison between the oscillation amplitude of the tip in terms of z_c for different situations of crack in the cantilever.

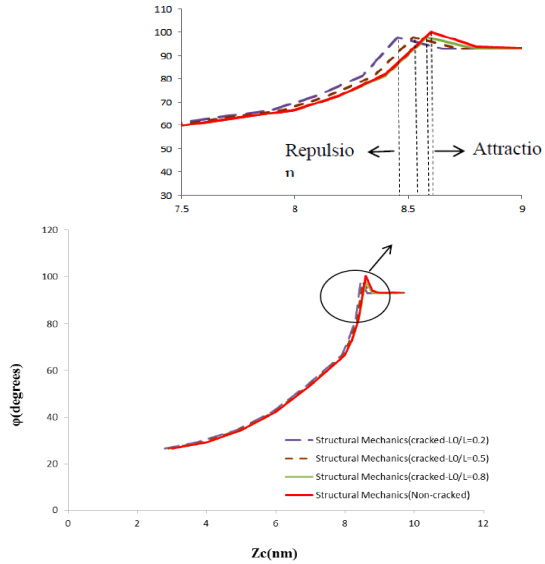

Fig.13
Comparison between the phase shifts in terms of z_c for different situations of crack in the cantilever.

The comparison of results of the present model with the results belonging to the molecular dynamics simulation indicates that although the general trend of results is in a good agreement, the oscillation amplitude values obtained from the structural mechanics model are very higher than that of the molecular dynamics results. Usually, in the molecular dynamics simulation, only the end of the microscope tip is atomically simulated, and the microscope tip is even simulated with very smaller radiuses compared to the experimental tests due to time limitations. Moreover, in some cases, there is a need for natural frequencies in the *GHz* range to cover the atomic vibration and prevent instability in the contact of the tip and sample, while AFMs in real conditions work with natural frequencies in the range of *kHz*. Therefore, the oscillation amplitude values obtained from the molecular dynamics simulation are less than those of the experimental tests.

The cantilever and the tip are simultaneously simulated in the structural mechanics model due to atomic-continuous simulation. Therefore, the tip of the microscope is simulated in real size. According to that the total van der Waals force is proportional to the radius of the tip, the bigger tip apex indicates the more interaction force between the tip and the sample. The tip modeling in its own real radius in the present model leads to covering all the tip-sample interactions, and as can be seen in Fig. 10 and Fig. 11, the results obtained from the present model have a good agreement with the experimental results.

4 CONCLUSION

In this paper, the vibrational behavior of the atomic force microscope on the graphene sample was simulated using a structural mechanics model and finite element method. The graphene sheet and the tip apex of the AFM were simulated using the structural mechanics model and the cantilever and the end part of the tip were simulated using the continuum model. In the structural mechanics model, the modified Morse, Lennard-Jones, and Tersoff potentials were used to model the interaction between atoms. Using multiscale models, one can employ the capability of atomic (high precision) and continuum (high speed) models simultaneously. The interaction between the silicon tip and graphene sheet was modeled by the Lennard-Jones nonlinear springs, and the contact behavior of the tip-sample was investigated by measuring the friction force during the tip movement on the sample. The results indicated that the friction force changes from 0.9 *nN* to 4.8 *nN* by increasing the radius of tip apex from 2.4 *nm* to 16 *nm*. Moreover, the reduction of the Poker effect initiated from increasing the number of graphene layers leads to reducing the friction force in a multilayer graphene so that the friction force decreases up to 12% by increasing each layer. The comparison of the structural mechanic model results with the molecular dynamics model and the experimental test indicated that the structural mechanics model is capable of predicting more real the AFM vibrational behavior. The molecular dynamics model cannot predict the real vibrational behavior of the cantilever because of the limitation in atomic complete modeling of the tip and cantilever and also the inability of its combination with the finite element continuous model as a result of a difference in time steps. Although this model can present acceptable results in the simulation of the contact behavior interatomic interactions in AFM and help to comprehend the nanoscale mechanisms, the study of the cracked cantilever showed that the crack, especially when it is close to the support, can dramatically affect the AFM vibration behavior.

REFERENCES

[1] Wang D., Russell T.P., 2018, Advances in atomic force microscopy for probing polymer structure and properties, *Macromolecules* **51**: 3-24.

[2] Qin Y., Brockett A., Ma Y., 2010, Micro-manufacturing: Research, technology outcomes and development issues, *The International Journal of Advanced Manufacturing Technology* **47**: 821-837.

[3] Ding S. Y., Yi J., Li J. F., 2016, Nanostructure-based plasmon-enhanced Raman spectroscopy for surface analysis of materials, *Nature Reviews Materials* **1**: 1-16.

[4] Li Z., Yan Y., Wang J., 2020, Molecular dynamics study on tip-based nanomachining: A review, *Nanoscale Research Letters* **15**: 1-12.

[5] Garcia R., 2020, Nanomechanical mapping of soft materials with the atomic force microscope: methods, theory and applications, *Chemical Society Reviews* **49**: 5850-5884.

[6] Misra S., Dankowicz H., Paul M. R., 2008, Event-driven feedback tracking and control of tapping-mode atomic force microscopy, *Proceedings of the Royal Society A: Mathematical, Physical and Engineering Sciences* **464**: 2113-2133.

[7] Tusset A. M., Bueno A. M., Nascimento C. B., 2013, Nonlinear state estimation and control for chaos suppression in MEMS resonator, *Shock and Vibration* **20**: 749-761.

[8] Bahrami M. R., 2020, Dynamic analysis of atomic force microscope in tapping mode, *Vibroengineering Procedia* **32**: 13-19.

[9] Dankowicz H., 2006, Nonlinear dynamics as an essential tool for non-destructive characterization of soft nanostructures using tapping-mode atomic force microscopy, *Philosophical Transactions of the Royal Society A: Mathematical, Physical and Engineering Sciences* **364**: 3505-3520.

[10] Rodrigues K. S., Balthazar J. M., Tusset A. M., 2014, Preventing chaotic motion in tapping-mode atomic force microscope, *Journal of Control, Automation and Electrical Systems* **25**: 732-740.

[11] Stark R. W., Schitter G., Stark M., 2004, State-space model of freely vibrating and surface-coupled cantilever dynamics in atomic force microscopy, *Physical Review B* **69**: 085412.

[12] Payam A. F., Fathipour M., 2009, Modeling and dynamic analysis of atomic force microscope based on Euler-Bernoulli beam theory, *Digest Journal of Nanomaterials and Biostructures* **4**: 565-578.

[13] Hsu J. C., Lee H. L., Chang W. J., 2007, Flexural vibration frequency of atomic force microscope cantilevers using the Timoshenko beam model, *Nanotechnology* **18**: 285503.

[14] Damircheli M., Korayem M. H., 2014, Dynamic analysis of AFM by applying Timoshenko beam theory in tapping mode and considering the impact of interaction forces in a liquid environment, *Canadian Journal of Physics* **92**: 472-483.

[15] Claeyssen J. R., Tsukazan T., Tonetto L., 2013, Modeling the tip-sample interaction in atomic force microscopy with Timoshenko beam theory, *Nanoscale Systems: Mathematical Modeling, Theory and Applications* **2**: 124-144.

[16] Espinoza-Beltrán F. J., Geng K., Muñoz Saldaña J., 2009, Simulation of vibrational resonances of stiff AFM cantilevers by finite element methods, *New Journal of Physics* **11**: 083034.

[17] Mendels D.A., Lowe M., Cuenat A., 2006, Dynamic properties of AFM cantilevers and the calibration of their spring constants, *Journal of Micromechanics and Microengineering* **16**: 1720-1733.

[18] Wang B., Wu X., Gan T. H., 2014, Finite element modelling of atomic force microscope cantilever beams with uncertainty in material and dimensional parameters, *Engineering Transaction* **62**: 403-421.

[19] Rodrigues K. S., Trindade M. A., 2018, Finite element modeling and analysis of an atomic force microscope cantilever beam coupled to a piezoceramic base actuator, *Journal of the Brazilian Society of Mechanical Sciences and Engineering* **40**: 427.

[20] Hu X., Egberts P., Dong Y., 2015, Molecular dynamics simulation of amplitude modulation atomic force microscopy, *Nanotechnology* **26**: 235705.

[21] Hu X., Chan N., Martini A., 2017, Tip convolution on HOPG surfaces measured in AM-AFM and interpreted using a combined experimental and simulation approach, *Nanotechnology* **28**: 025702.

[22] Kim H., Venturini G., Strachan A., 2012, Molecular dynamics study of dynamical contact between a nanoscale tip and substrate for atomic force microscopy experiments, *Journal of Applied Physics* **112**: 094325.

[23] Onofrio N., Venturini G. N., Strachan A., 2013, Molecular dynamic simulation of tip-polymer interaction in tapping-mode atomic force microscopy, *Journal of Applied Physics* **114**: 094309.

[24] Ye Z., Tang Ch., Dong Y., 2012, Role of wrinkle height in friction variation with number of graphene layers, *Journal of Applied Physics* **112**: 116102.

[25] Dou Z., Qian J., Li Y., 2020, Molecular dynamics simulation of bimodal atomic force microscopy, *Ultramicroscopy* **212**: 112971.

[26] Lee H. L., Chang W.J., 2012, Sensitivity analysis of a cracked atomic force microscope cantilever, *Japanese Journal of Applied Physics* **51**: 035202.

[27] Lee H. L., Chang W. J., 2012, Dynamic response of a cracked atomic force microscope cantilever used for nanomachining, *Nanoscale Research Letters* **7**: 131.

[28] Chang W.J., Lee H.L., Yang Y.C., 2015, Free vibration analysis of a cracked atomic force microscope cantilever, *Proceedings of the World Congress on New Technologies*, Barcelona, Spain.

[29] Dastjerdi Sh., Abbasi M., 2019, A vibration analysis of a cracked micro-cantilever in an atomic force microscope by using transfer matrix method, *Ultramicroscopy* **196**: 33-39.

[30] Stuart S.J., Tutein A.B., Harrison J. A., 2000, A reactive potential for hydrocarbons with intermolecular interactions, *The Journal of Chemical Physics* **112**: 6472-6486,

[31] Ong Z.Y., Pop E., 2010, Molecular dynamics simulation of thermal boundary conductance between carbon nanotubes and SiO2, *Physical Review B* **81**: 155408.

[32] Neek-Amal M., Peeters F., 2010, Nanoindentation of a circular sheet of bilayer graphene, *Physical Review B* **81**: 235421.

[33] Yoon H.M., Jung Y., Jun S.C., Kondaraju S., Lee J.S., 2015, Molecular dynamics simulations of nanoscale and subnanoscale friction behavior between graphene and a silicon tip: Analysis of tip apex motion, *Nanoscale* **7**: 6295-6303.

[34] Garcıa R., Perez R., 2002, Dynamic atomic force microscopy methods, *Surface Science Reports* **47**: 197-301.

[35] Vahdat V., Grierson D.S., Turner K.T., Carpick R.W., 2011, Nano-scale forces, stresses, and tip geometry evolution of amplitude modulation atomic force microscopy probes, *ASME 2011 International Design Engineering Technical Conferences and Computers and Information in Engineering Conference* (*American Society of Mechanical Engineers*).